Edelweiss Applied Science and Technology
ISSN: 2576-8484
Vol. 9, No. 2, 2208-2223
2025
Publisher: Learning Gate
DOI: 10.55214/25768484.v9i2.5058

Radiation shielding properties of xPbF2−20Na2O−10CaO−(70−x) B2O3 glass system

Abdalla A.S. Esmail[1*], Kassab M.M[1], Radwan M.M[1], A. Abd-Latif M[1,2]
[1]Dept. of Mathematics and Engineering Physics, Faculty of Engineering, Fayoum University, Egypt; asb11@fayoum.edu.eg (A.A.E.).
[2]Dept. of Basic science, Faculty of Dentistry, Al-Ryada University for Science and Technology, Egypt.

Abstract: The influence of PbF2 incorporation on the physical and radiation shielding properties of six glass samples, labeled BPbF0 to BPbF25, was investigated. These samples have a composition of xPbF2−20Na2O−10CaO−(70−x) B2O3 where (0≤x≤25 in 5 mol.% increments). The physical parameters, including density and molar volume, were calculated. As PbF2 content increased, the density rose significantly from 2.476 g/cm³ to 4.077 g/cm³, attributed to the substitution of low molecular weight B2O3 with high molecular weight PbF2. Similarly, the molar volume increased from 26.95 cm³/mol to 27.138 cm³/mol, indicating the formation of non-bridging oxygen atoms and the expansion of the glass network. X-ray diffraction (XRD) analysis confirmed the amorphous nature of the samples, as no crystalline peaks were observed. Gamma radiation shielding parameters were theoretically evaluated using Phys-X/PSD software. The mass attenuation coefficient (MAC) and linear attenuation coefficient (LAC) were found to increase with higher PbF2 content at a given energy. Both coefficients decreased linearly between 0.015 and 0.08 MeV with increasing energy, remained nearly constant in the range of 1 to 3 MeV due to Compton scattering, and increased gradually beyond 3 MeV due to pair production. The half-value layer (HVL) and mean free path (MFP) decreased as PbF2 content increased, reflecting improved shielding efficiency. Furthermore, the effective atomic number (Zeff) and effective neutron density (Neff) also increased with higher PbF2 content. Compared to commercial glasses like RS-360 and various concretes, the prepared glass system demonstrated superior gamma-ray shielding properties. These findings suggest that the developed glass system is highly effective for gamma radiation shielding applications.

Keywords: *Effective electron density (Neff), Exposure buildup factor (EBF) gamma shielding, Half value layer thickness (HVL), Lead fluoride borate glass, Mass attenuation coefficient.*

1. Introduction

The leakage of gamma radiation from nuclear reactors poses a serious hazard due to its ability to travel long distances through the air, penetrate various materials, and cause indirect ionization. Gamma rays represent a significant long-term danger in nuclear disasters, as evidenced by the catastrophes at Fukushima Daiichi and Chernobyl. Workers handling radioactive materials or laboratory equipment are particularly at risk of overexposure to different forms of radiation. High doses of gamma radiation can lead to severe health consequences, including radiation sickness, cancer, bone marrow depletion, and even death. Consequently, research on effective gamma radiation protection has become increasingly critical.

Effective radiation protection relies on adequate shielding to minimize exposure from the radiation source. Among shielding materials, concrete is the most commonly used in nuclear reactors due to its

History: Received: 30 December 2024; Revised: 24 January 2025; Accepted: 19 February 2025; Published: 26 February 2025
* Correspondence: asb11@fayoum.edu.eg

affordability, availability, and adaptability to various shapes and sizes. However, concrete has notable limitations:

1. Cracking over time: Prolonged use can lead to the formation of cracks, reducing its effectiveness.
2. Water content issues: The presence of water in concrete lowers its density and structural strength.
3. Thermal effects: Exposure to nuclear radiation causes heating, resulting in water loss and structural degradation, which introduces uncertainties in shielding parameters.
4. Lack of portability: Concrete is heavy and difficult to transport.
5. Opacity: Its lack of transparency limits its use in applications requiring visibility.

Given these limitations, exploring alternative shielding materials is essential. Options such as alloys, steel, polymers, clay, gemstones, and glass offer promising solutions. For specific applications like reactor windows and nuclear waste containers, glass stands out as an ideal choice. Its transparency enables visibility, and its shielding performance can be significantly enhanced by incorporating heavy metal oxides.

One of the most effective types of shielding glass is lead-doped borate glass. This material combines the benefits of high density and a high atomic number, making it an excellent choice for improving radiation protection.

There are many researches about lead borate glass in form of borate glass doped with lead oxide such as (PbO-Na_2O-B_2O_3) [1] ($xPbO$:(100− x) +B_2O_3) [2] (xBi_2O_3+(0.8-x)PbO+0.2B_2O_3) [3] (50B_2O_3–10ZnO –(40-x)Pb_3O_4) + x La_2O_3) [4] and (60B_2O_3+Pb3O4+(20-x)ZnO + xWO_3); and in form of borate glass doped with lead fluoride such as (PbF_2-TeO_2-B_2O_3-Eu_2O_3) [5] ((25-x)PbF_2-xCaF_2-0.2Cr_2O_3–25Bi_2O_3–49.8B_2O_3–) [6] (55B_2O_3-(45-x)PbF_2-BaF_2) [7] and((25-x)PbF_2-xZnF_2-0.2Cr_2O_3 - 25Bi_2O_3- 49.8 B_2O_3-) [8]. Furthermore, RS-360 glass (containing 45 wt% PbO) which is a commercial glass used in shielding windows

Lead fluoride borate glass offers several advantages over other types of glass. Its high refractive index allows it to bend light more effectively, making it ideal for lenses and various optical components. Additionally, its exceptional transparency in the infrared region of the electromagnetic spectrum makes it highly valuable for applications in infrared optics and optical fibers.

This glass also demonstrates excellent chemical and thermal resistance, enhancing its durability in demanding environments. Furthermore, its relatively low melting point simplifies manufacturing and molding processes, enabling the creation of precise shapes. Lead fluoride borate glass can be molded, polished, and coated to produce lenses, prisms, waveguides, and numerous other optical components [7, 9].

The unique combination of properties in lead fluoride borate glass makes it suitable for a broad range of applications. Its superior optical characteristics are especially advantageous for high-quality lenses used in cameras, microscopes, and telescopes. However, because it contains lead—a toxic heavy metal—it is essential to implement strict safety measures during its production, use, and disposal to mitigate associated health and environmental risks [8, 9].

In this study, a system of lead fluoride borate glass was proposed for nuclear shielding applications. The glass composition was defined as $xPbF_2$: 10 CaO: 20 Na_2O: (70-x) B_2O_3 where X = 0%:5%:25% mole. Boron oxide (B_2O_3) was used as the primary glass former due to its exceptional chemical and thermal stability [2]. Sodium oxide (Na_2O) was included to expand the glass-forming range, facilitate ion exchange, and lower the melting point, further optimizing the material for practical applications.

2. Materials and Methods

2.1. Samples Preparation

We used melt quenching technique to prepare the glass samples which labeled as, BPbF0, BPbF5, BPbF10, BPbF15, BPbF20 and BPbF25, of glass system of $xPbF_2$: 10 CaO: 20 Na_2O: (70-x) B_2O_3 where (x=0: 5%: 25%) mole.

Edelweiss Applied Science and Technology
ISSN: 2576-8484
Vol. 9, No. 2: 2208-2223, 2025
DOI: 10.55214/25768484.v9i2.5058

During the preparation of the batch, high-purity analytical-grade chemicals (DOP ORGANIK, Turkey) were used, including H_3BO_3 (61.83 g/mol), $CaCO_3$ (100.0869 g/mol), NaOH (39.997 g/mol), and PbF_2 (245.2 g/mol). The chemicals were weighed accurately, ground, and mixed thoroughly using a mortar and pestle for approximately 30 minutes to ensure uniformity.

The prepared mixture was preheated to approximately 300°C and then quenched using copper molds and plates. A 30 g batch of the starting materials was melted at 950°C for 40 minutes in a porcelain crucible placed in an electric furnace (MT1210-LU, China) with a controlled heating rate of 5°C/min. After melting, the mixture was rapidly cooled to room temperature.

To alleviate mechanical stresses typically introduced during the melting process, the samples were transferred to a different crucible and annealed at 400°C for 5 hours in a separate furnace. This annealing step ensures improved structural stability and quality of the final material.

2.1.1. Density Measurement and Related Parameters

The density (ρ) and molar volume (V_M) are measured to analyze the structural properties of the material. These parameters serve as valuable indicators of structural changes, as they are influenced by factors such as structural softness, compactness, and cross-linking.

Density is determined using Archimedes' principle, with xylene employed as the buoyant liquid. The samples are first weighed in air and then in xylene using a precise electronic scale. The density (ρ) is calculated using the following equation:

$$\rho = \frac{w_a}{w_a - w_l}\rho_l \quad (1)$$

where w_a the weight of the sample in air,
w_l is the weight of the sample in Xylene,
ρ_l the Xylene density which is 0.8630 g/cm^3
Molar volume (V_M) of the prepared glasses were calculated using the following equations:

$$V_m = \frac{\sum x_i M_i}{\rho} = \frac{M_w}{\rho} \quad (2)$$

where ρ, M_i , x_i and M_w are the glass density, the molecular weight and molar fraction of each component i , and the total molecular weight of the sample, respectively [10-12].

2.2. Radiation Shielding Parameters: Theoretical Formulae

Experimental and simulation techniques are widely employed to evaluate the shielding The effectiveness of materials in radiation shielding is often assessed using a combination of experimental and simulation techniques. Simulations are particularly valuable for predicting shielding performance and validating experimental findings. They also enable optimization of material compositions before production, improving attenuation properties. Previous research has consistently demonstrated the reliability of simulations in evaluating material characteristics.

In this study, shielding coefficients, including the linear attenuation coefficient (LAC, μ), the mass attenuation coefficient (MAC, μ_m), the half-value layer (HVL) thickness of the glass, and the exposure buildup factor (EBF), were calculated theoretically. These calculations were performed using the PHY-X/PSD software [13] which applies well-established theoretical formulae.

2.2.1. Gamma Radiation Shielding Attenuation Coefficients

The shielding prameters of the produced glass were theoretically analyzed using Phy-X/PSD software across a continuous gamma energy range from 0.01 to 15 MeV [13]. Lambert-Beer's law is used to calculate the Linear attenuation coefcient [14-22].

Edelweiss Applied Science and Technology
ISSN: 2576-8484
Vol. 9, No. 2: 2208-2223, 2025
DOI: 10.55214/25768484.v9i2.5058

$$\mu = \ln\left(\frac{I}{I_0}\right)/d \tag{3}$$

where I(the transmitted photon energy), I_0(photon energy of the incoming radiation), and d (the thickness of the glass). The μ_m is calculated by this formula [12, 15].

$$\mu_m = \left(\frac{\mu}{\rho}\right)_c = \sum_i w_i \left(\frac{\mu}{\rho}\right)_i \tag{4}$$

where ρ_i is the ith constituent's partial density, $\frac{\mu}{\rho}$ is the ith constituent's mass attenuation and w_i is the ith constituent's weight fraction.

The mean free path (MFP), measured in centimeters, is the reciprocal of the linear attenuation coefficient. It illustrates how gamma photons interact with the glass system and indicates the material's effectiveness in providing shielding [14-22].

$$MFP = \frac{1}{\mu} \tag{5}$$

2.2.2. Effective Atomic Number Z_{eff} and Effective Electron Density N_{eff}.

The effective atomic number (Z_{eff}) is very important for determining photon interaction with matter. The atomic number of a composite material cannot be represented as a single number. It can be calculated using the formula below [12, 19, 23].

$$Z_{eff} = \frac{\sum_i f_i A_i (\frac{\mu}{\rho})_i}{\sum_i \frac{f_i A_i}{Z_i} (\frac{\mu}{\rho})_i} \tag{6}$$

Where $\left(\frac{\mu}{\rho}\right)_i$ are the ith element's mass attenuation coefficient f_i is the fraction of atoms of the ith element relative to the total number of atoms in the mixture, A_i refers to the atomic weight (in grams) of the ith element and Z_i corresponds to its atomic number.

The effective electron density (N_{eff}) can be calculated by:

$$N_{eff} = N_A \frac{Z_{eff}}{\sum f_i A_i} \tag{8}$$

Where N_A is Avogadro's number.

2.2.3. Energy Exposure Buildup Factor (EBF)

Calculating the buildup factor is essential for designing and manufacturing effective radiation shielding materials. This factor accounts for secondary radiation and scattered photons, providing a corrected response for un-collided photons. While the Lambert-Beer law is often too simplistic and only accurate under specific conditions, its accuracy improves when the buildup factor is incorporated as a corrective measure. This parameter is always equal to or greater than unity and is applied in the modified Lambert-Beer law [24, 25].

Buildup factors are typically classified into two types: the exposure buildup factor (EBF) and the energy absorption buildup factor (EABF). The EABF quantifies the energy deposited or absorbed within the shielding material and detected by the absorber. Conversely, the EBF represents the buildup

Edelweiss Applied Science and Technology
ISSN: 2576-8484
Vol. 9, No. 2: 2208-2223, 2025
DOI: 10.55214/25768484.v9i2.5058

factor associated with the exposure response of the detector. Both factors are influenced by various parameters, including atomic number, absorber thickness, photon energy, geometry, attenuation coefficient, and mean free path [24, 25].

The geometric progression (G-P) fitting method is widely recognized as the most reliable and precise approach for calculating buildup factor values, as supported by extensive research. Originally introduced by Harima [26]; Harima [27] and Harima, et al. [28] this method has been shown to align closely with results from the PALLAS program. In this study, the G-P fitting method was employed to calculate the EABF and EBF for the developed lead fluoride borate glasses. These calculations were performed across photon energy levels ranging from 0.015 to 15 MeV and for penetration depths of up to 40 mean free paths.

The formula below is used to calculate EBF of the glass by G-P fitting parameters [29]:

$$B(E,X) = 1 + \frac{b-1}{K-1}(K^x - 1) \qquad \text{For K} \neq 1 \qquad (9)$$

$$B(E,X) = 1 + (b-1)x \qquad \text{For K} = 1 \qquad (10)$$

Where,

$$K(E,x) = cx^a + d\frac{\tanh\left(\frac{x}{X_k} - 2\right) - \tanh(-2)}{1 - \tanh(-2)} \qquad for\ x \leq 40\ mfb \qquad (11)$$

where E is the incident photon energy, x is the penetration depth in mfp, and a, b, c, d and X_k are the G-P fitting parameters.

3. Results and Discussion

3.1. Physical Properties

The density of the prepared glass and molar volume are listed in *Table 1* below. Figure 1 shows the variation of density (ρ) of the glass and molar volume (V_m) with PbF_2. As the PbF_2 content increases at the expense of B_2O_3 oxide, the glass density rises from 2.481 to 4.077 g/cm³, and the glass molar volume increases from 26.950 to 27.138 cm³/mol. This rise in density is attributed to the substitution of B_2O_3, with a molecular weight of 69.62 g/mol and a density of

2.46 g/cm³, by PbF_2, which has a significantly higher molecular weight of 245.196 g/mol and a density of 8.445 g/cm³. The overall density of the glass system increases as B_2O_3 is replaced by the higher molecular weight PbF_2.

Table 1.
The Density and the molar volume of the glass samples.

Sample	Density (ρ) (g/cm³)	Molar volume V_m (cm³/mole)
BPbF0	2.4760	26.9500
BPbF5	2.7980	26.9880
BPbF10	3.1190	27.0250
BPbF15	3.4390	27.0630
BPbF20	3.7580	27.1000
BPbF25	4.0770	27.1380

The molar volume of glass is influenced by changes in its structural arrangement. As a parameter directly related to bond length, molar volume plays a critical role in understanding the glass properties during the experimental process. The observed increase in molar volume of the prepared glasses, from 26.950 to 27.138 cm³/mol, although the increasing in the density, is attributed to the larger atomic

Edelweiss Applied Science and Technology
ISSN: 2576-8484
Vol. 9, No. 2: 2208-2223, 2025
DOI: 10.55214/25768484.v9i2.5058

radius of lead atoms (202 pm) compared to boron atoms (192 pm). This difference in atomic size affects the bond length of Pb–O within the glass network, resulting in the expansion of the molar volume [30].

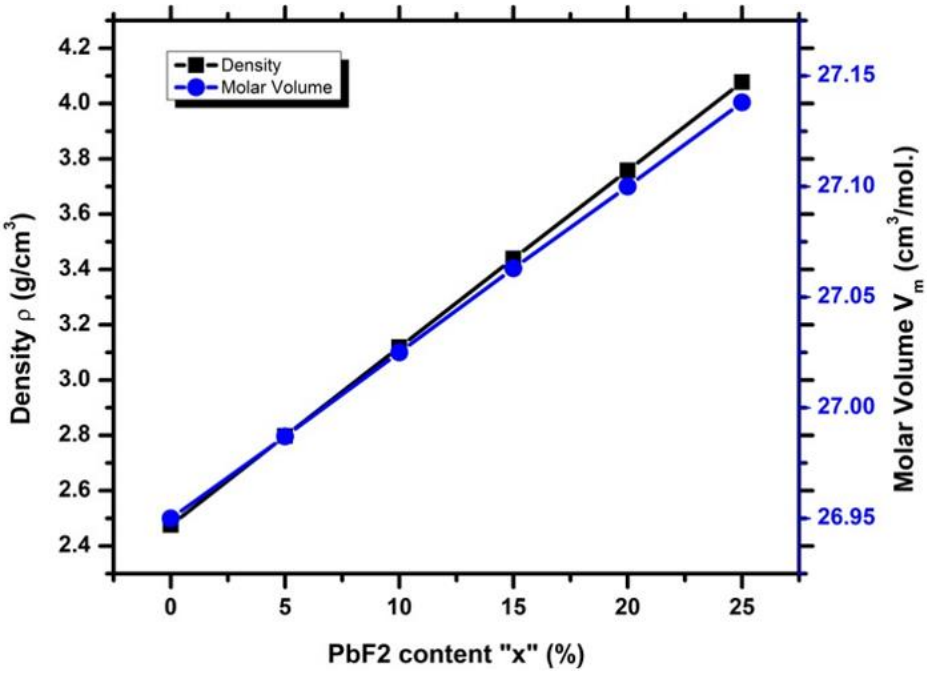

Figure 1.
Glass Density (ρ) and the Molar Volume (V_m) VS the PbF_2 content (%).

3.2. X-Ray Diffraction Spectra

The XRD spectra for all the prepared glasses were measured from 10^o-70^o as shown in Figure 2, it confirms the glass is in amorphous structure with absence of any sharp peaks that might be in the crystalline structure.

Edelweiss Applied Science and Technology
ISSN: 2576-8484
Vol. 9, No. 2: 2208-2223, 2025
DOI: 10.55214/25768484.v9i2.5058

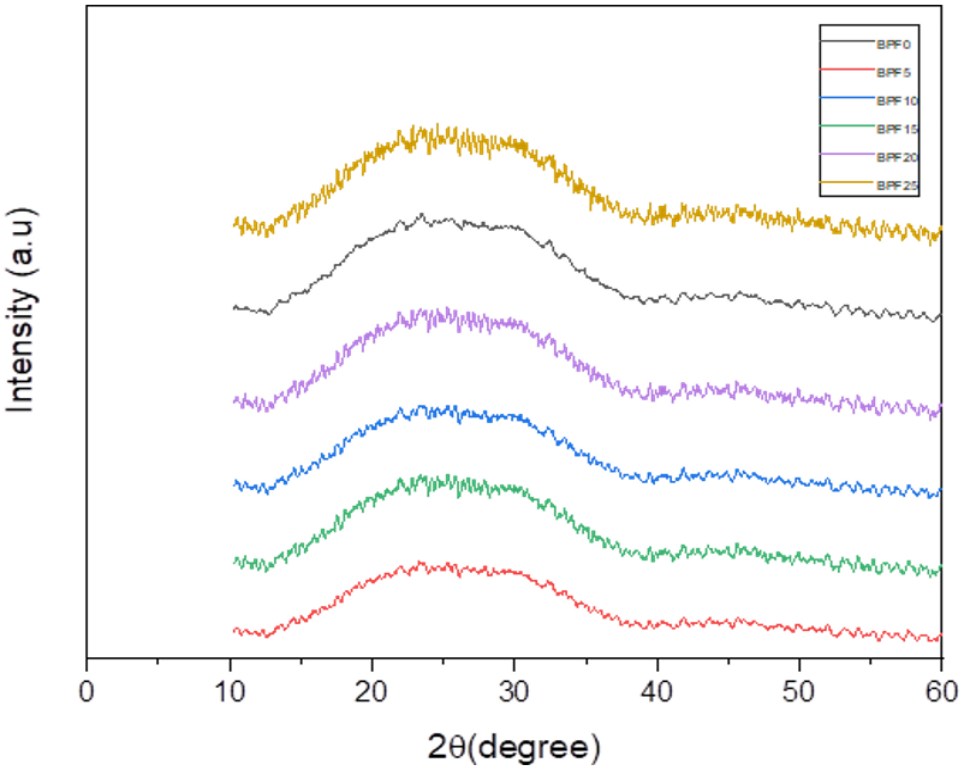

Figure 2.
XRD Spectra of all Samples.

3.3. Radiation Shielding Properties

(i) Linear attenuation coefficient (LAC) (μ)and Mass attenuation coefficients (MAC) (μ_m).

The mass attenuation coefficient (MAC), μ_m , for the produced glass samples is plotted against the photon energy of the incoming radiation in Figure 3. The maximum MAC for all samples is observed at low energy (0.015 MeV). As the PbF_2 content increases, the MAC decreases linearly in the energy range of 0.015 to 0.08 MeV. A sharp peak in MAC is observed at 0.1 MeV, corresponding to the K-edge absorption energy of lead. In the energy range of 1.0 to 3.0 MeV, the μ_m values remain nearly constant, which can be attributed to the Compton scattering effect. Beyond 3 MeV, the μ_m values gradually increase due to the pair production process. Notably, the BPbF25 sample exhibits the highest MAC value.

Similarly, the variation of the linear attenuation coefficient (LAC) with photon energy is plotted in Figure 4. The LAC follows a pattern similar to that of the MAC, with higher PbF_2 concentrations leading to increased LAC values.

Edelweiss Applied Science and Technology
ISSN: 2576-8484
Vol. 9, No. 2: 2208-2223, 2025
DOI: 10.55214/25768484.v9i2.5058

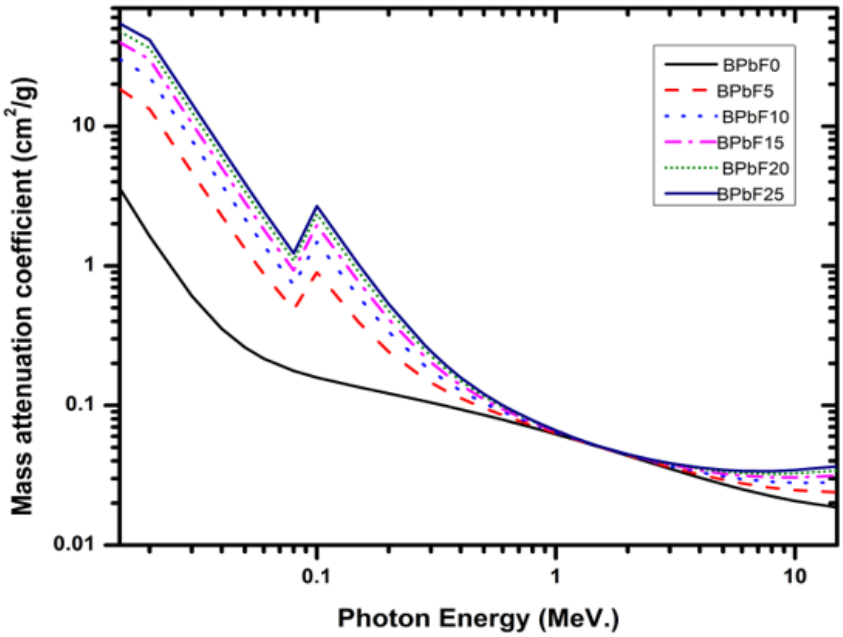

Figure 3.
Changing of the mass attenuation coefficient (MAC) μ_m, versus the photon energy of the incoming radiation for the prepared lead fluoride borate glass.

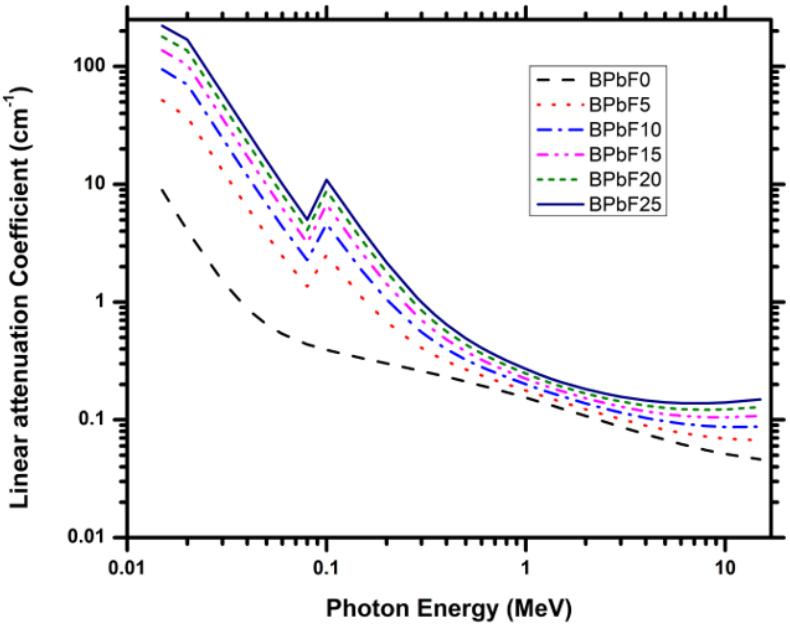

Figure 4.
Changing of the linear attenuation coefficient(LAC) μ, versus the photon energy of the incoming radiation energy for the prepared lead fluoride borate glass.

Edelweiss Applied Science and Technology
ISSN: 2576-8484
Vol. 9, No. 2: 2208-2223, 2025
DOI: 10.55214/25768484.v9i2.5058

(ii) Half-value layer (HVL), and mean free path (MFP)

The half-value layer (HVL) of the studied glass samples is presented in Figure 5. As the energy increases up to 6 MeV, the HVL values for all samples also increase. Beyond 6 MeV, the HVL values remain relatively constant. Within the energy range of 0.015 to 15 MeV, increasing the PbF_2 content results in a decrease in the HVL of the glass samples. Figure 5 highlights that the BPbF25 glass sample ($25PbF_2$-$20Na_2O$-$10CaO$-$45B_2O_3$) exhibits the lowest HVL.

Figure 6 illustrates the variation of the mean free path (MFP) with the photon energy of the incoming radiation. The MFP increases as the photon energy rises within the range of 0.015 to 15 MeV. Among the samples, BPbF25, which has the highest PbF_2 content, demonstrates the lowest MFP.

Figure 7 depicts the variation of the mean free path (MFP) with lead fluoride (PbF_2) content at different energy levels. The shielding effectiveness of the glass material against gamma radiation can be assessed using the HVL and MFP values. Glass with lower HVL and MFP values offers enhanced protection. In this context, the BPbF25 sample demonstrates superior shielding performance.

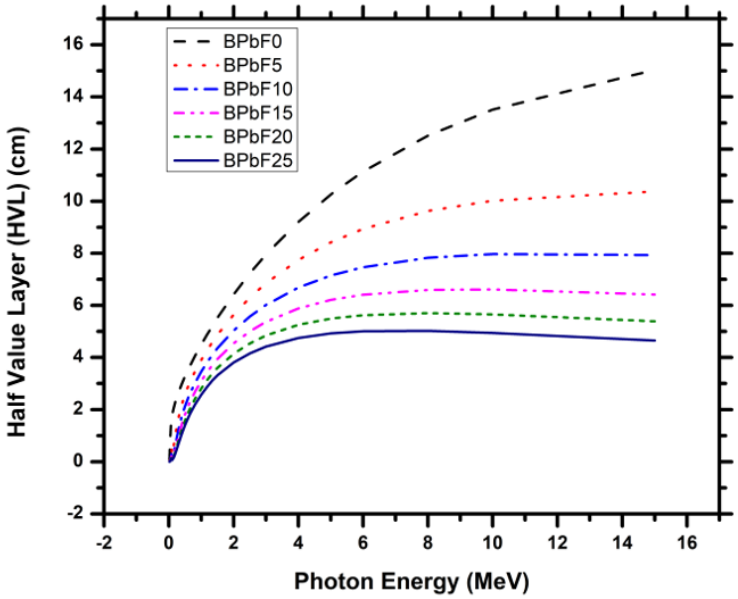

Figure 5.
Changing of the (HVL), with the photon energy of the incoming radiation energy for the prepared lead fluoride borate glass

Edelweiss Applied Science and Technology
ISSN: 2576-8484
Vol. 9, No. 2: 2208-2223, 2025
DOI: 10.55214/25768484.v9i2.5058

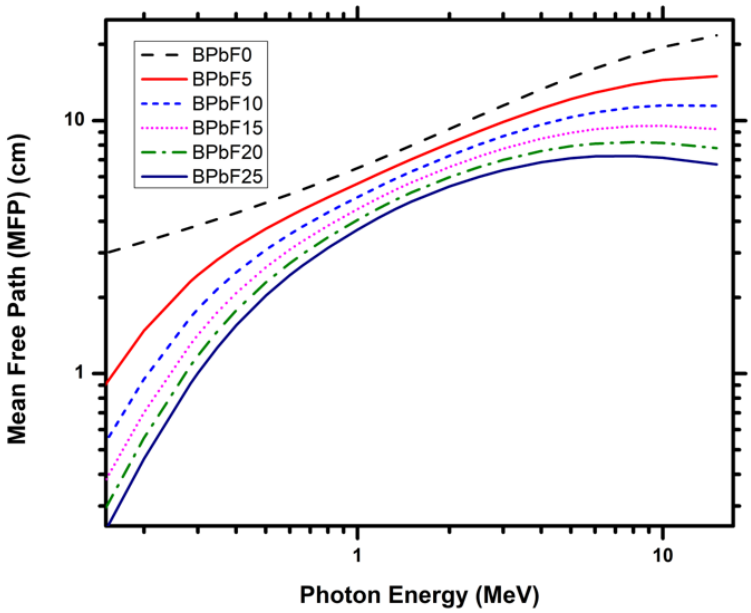

Figure 6.
Changing of the (MFP), with the photon energy of the incoming radiation energy for the prepared lead fluoride borate glass.

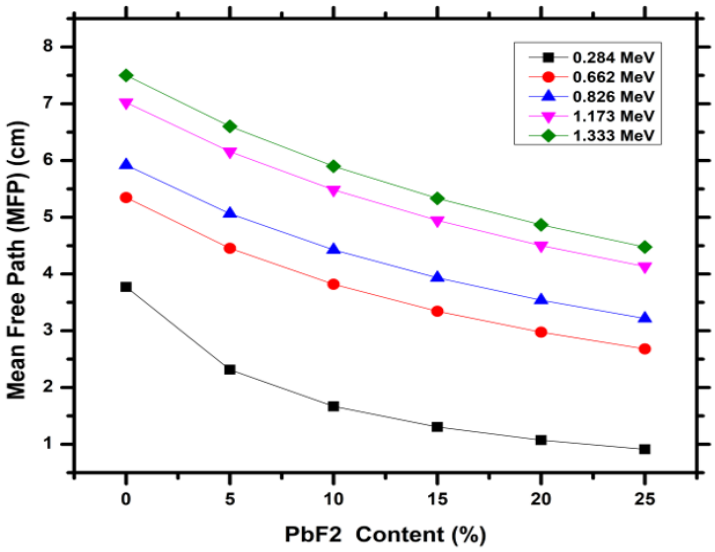

Figure 7.
Changes of the (MFP) with varying PbF2 content across different energy levels.

(iii) Effective atomic number (Zeff) and effective electron density (Neff)

The calculated Effective atomic number (Z_{eff}) and Effective electron density (N_{eff}) values as functions of photon energy for the ($xPbF_2$-20Na_2O-10CaO-(70−x)B_2O_3) glass system are presented in Figures 8 and 9, respectively. These plots reveal that all glass samples exhibit a pea Z_{eff} value at very low photon energies (~0.02 MeV). Similar trends observed in the μ_m and Z_{eff} spectra suggest that Z_{eff} can serve as an indicator of the photon shielding capabilities of these glasses. The Z_{eff} values of the prepared glasses

Edelweiss Applied Science and Technology
ISSN: 2576-8484
Vol. 9, No. 2: 2208-2223, 2025
DOI: 10.55214/25768484.v9i2.5058

increase with the substitution of B_2O_3 by PbF_2 and decrease with rising photon energy. This behavior highlights those materials with a higher weight fraction of high atomic number (Z) elements, such as lead (Pb), exhibit greater Z_{eff} values. Specifically, the higher Pb content and resulting increased density contribute significantly to the high effective atomic number observed in the BPbF25 sample.

Figure 9 illustrates the variation of the effective electron density (N_{eff}) with photon energy. In the low-energy range, where photoelectric absorption predominates, samples with lower PbF_2 content exhibit higher N_{eff} values. Conversely, in the energy range 1.0 MeV≤E≤3.0 MeV, where Compton scattering dominates N_{eff} remains constant across all samples. This indicates that, within this energy range N_{eff} is independent of the chemical composition of the glass.

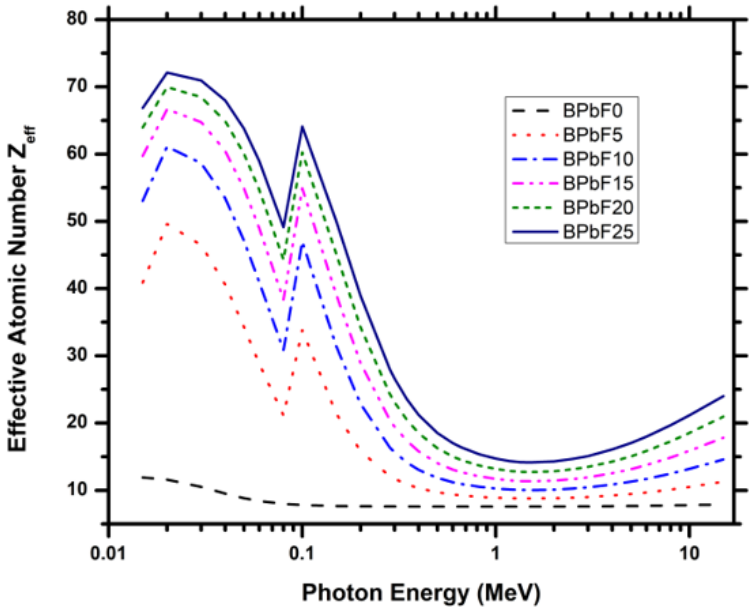

Figure 8.
Changing of the effective atomic number Z_{eff}, with the incident photon energy for the prepared lead fluoride borate glass.

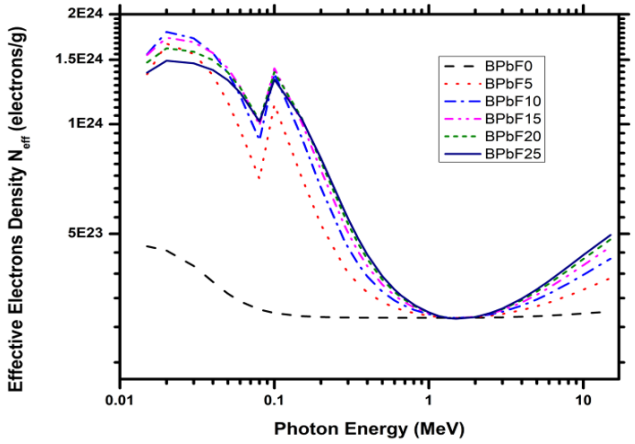

Figure 9.
Changing of N_{eff}, with the photon energy of the incoming radiation energy for

Edelweiss Applied Science and Technology
ISSN: 2576-8484
Vol. 9, No. 2: 2208-2223, 2025
DOI: 10.55214/25768484.v9i2.5058

Table 2.
Different Radiation parameters of the glass samples at (284, 347,662, 826, 1173, and 1333 keV) photon energies of Cs^{137} and Co^{60}

Sample code	Photon Energy (KeV)	Mass attenuation coefficient (μ_m) (cm^2/g)	Linear attenuation coefficient(μ) cm^{-1}	HVL (cm)	TVL (cm)	MFP (cm)	Zeff
BPbF0	284	0.107	0.265	2.614	8.684	3.771	7.6
	347	0.099	0.245	2.826	9.388	4.077	7.590
	662	0.076	0.187	3.705	12.309	5.346	7.590
	826	0.068	0.169	4.103	13.629	5.919	7.590
	1173	0.057	0.142	4.868	16.172	7.023	7.590
	1333	0.039	0.096	7.239	24.048	10.444	7.590
BPbF5	284	0.155	0.433	1.602	5.323	2.312	12.10
	347	0.127	0.355	1.954	6.492	2.819	10.90
	662	0.080	0.225	3.087	10.255	4.454	9.25
	826	0.071	0.197	3.510	11.659	5.063	9.03
	1173	0.058	0.162	4.268	14.178	6.157	8.83
	1333	0.054	0.151	4.576	15.201	6.602	8.80
BPbF10	284	0.192	0.600	1.156	3.841	1.668	16.37
	347	0.149	0.464	1.494	4.965	2.156	14.15
	662	0.084	0.262	2.647	8.792	3.818	10.95
	826	0.072	0.226	3.068	10.191	4.426	10.53
	1173	0.058	0.182	3.801	12.626	5.483	10.13
	1333	0.054	0.170	4.089	13.583	5.899	10.07
BPbF15	284	0.223	0.766	0.905	3.006	1.305	20.44
	347	0.166	0.573	1.210	4.021	1.746	17.34
	662	0.087	0.299	2.317	7.697	3.343	12.71
	826	0.074	0.254	2.725	9.053	3.932	12.07
	1173	0.059	0.202	3.427	11.383	4.944	11.49
	1333	0.055	0.188	3.696	12.279	5.333	11.39
BPbF20	284	0.248	0.932	0.744	2.470	1.073	24.31
	347	0.181	0.681	1.018	3.380	1.468	20.47
	662	0.089	0.336	2.061	6.847	2.974	14.52
	826	0.075	0.283	2.452	8.147	3.538	13.68
	1173	0.059	0.222	3.120	10.365	4.502	12.90
	1333	0.055	0.205	3.374	11.207	4.867	12.76
BPbF25	284	0.269	1.098	0.631	2.098	0.911	28.01
	347	0.194	0.789	0.878	2.917	1.267	23.55
	662	0.092	0.373	1.857	6.167	2.678	16.38
	826	0.076	0.311	2.230	7.407	3.217	15.34
	1173	0.059	0.242	2.865	9.517	4.133	14.37
	1333	0.055	0.223	3.103	10.309	4.477	14.20

The measured values for the mass attenuation coefficient (MAC), linear attenuation coefficient (LAC), half-value layer (HVL), mean free path (MFP), and effective atomic number (Z_{eff})various energy levels are summarized in Table 2. These values are further compared with those of other shielding materials, as shown in Table 3.

Table 3 lists the MAC, HVL, TVL, MFP, and Z_{eff} values for the $xPbF_2$-$20Na_2O$-10CaO-$(70-x)B_2O_3$ Glass system alongside:

i) Other prepared glasses, such as BTZ5 [15] G6 [19] and S25 [1];

ii) Commercially available shielding glasses (RS253 G18 and RS360) used as shielding window materials [18, 19];

iii) Common concretes, including ordinary and barite concretes [31].

The data reveal that the prepared glass sample BPbF25 exhibits superior MAC, HVL, and MFP values compared to both types of concrete and the RS253 G18 commercial glass. Additionally, samples

Edelweiss Applied Science and Technology
ISSN: 2576-8484
Vol. 9, No. 2: 2208-2223, 2025
DOI: 10.55214/25768484.v9i2.5058

with PbF_2 concentrations exceeding 20% outperform the RS360 commercial glass in shielding effectiveness.

Table 3.
Comparison of our glass system BPF25 with some glass systems at (662KeV) [1, 15, 18, 19] and some concretes [31].

Samplecode	Chemical composition(mol%)	Density(ρ) g/cm^3	Mass attenuation(μ/ρ) cm^2/g	MFP	HVL
BPbF0	70B_2O_3 +20 Na_2O + 10CaO + 0PbF_2	2.473	0.076	5.35	3.71
BPbF5	65B_2O_3 + 20Na_2O +10 CaO +5 PbF_2	2.798	0.080	4.45	3.09
BPbF10	60B_2O_3 + 20Na_2O +10 CaO +10 PbF_2	3.119	0.084	3.82	2.65
BPbF15	55B_2O_3 + 20Na_2O + 10CaO +15 PbF_2	3.439	0.087	3.34	2.32
BPbF20	50B_2O_3 +20 Na_2O + 10CaO + 20PbF_2	3.758	0.089	2.97	2.06
BPbF25	45B_2O_3 +20Na_2O + 10CaO +25 PbF_2	4.076	0.092	2.68	1.86
BTZ5	60B_2O_3 + 10Na_2O + 7CaO + 20TeO_2 +3ZrO_2	3.273	0.075	4.05	2.81
G6	25B_2O_3 + 10BaO + 65Bi_2O_3	4.942	0.097	2.08	1.45
S25	55B_2O_3 +20 Na_2O + 25PbO	3.77	0.092	2.88	1.50
RS 253G18	10B_2O_3 +70SiO_2 + 8Na_2O +2CeO_2+1BaO+9K_2O	2.53	0.075	5.27	3.65
RS 360	45SiO_2 + 9(Na_2O + K_2O) + 45PbO	3.6	0.088	3.16	2.19
Ordinary concrete		2.3	0.077	5.65	3.91
Barite concrete		3.5	0.078	3.66	2.53

(i) The energy buildup factors EBF

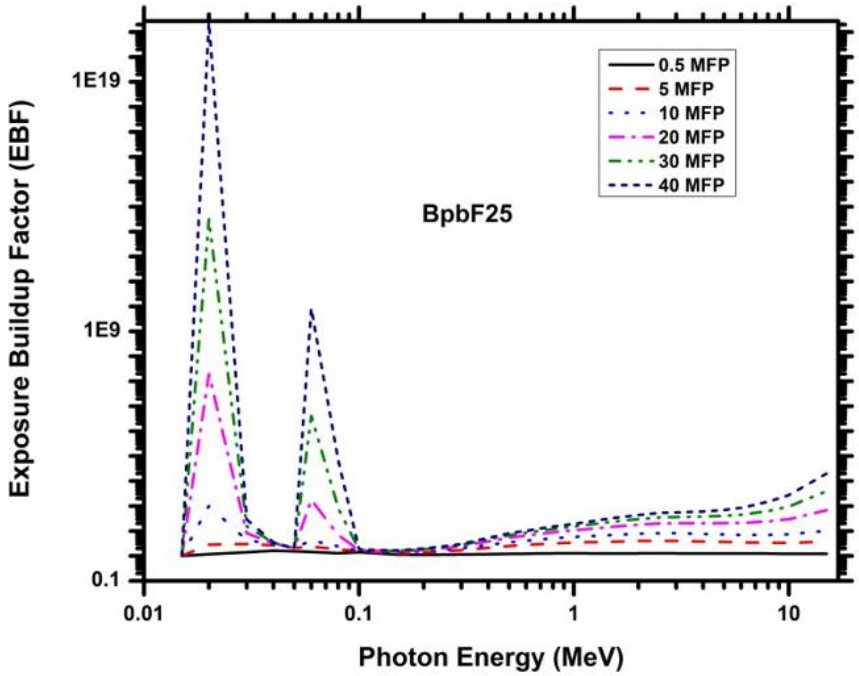

Figure 9.
EBF variation with the photon energy at different MFP of BPbF2 samples.

Figure 9 illustrates the changes in EBF changing with the photon energy for BPbF25 glass at

Edelweiss Applied Science and Technology
ISSN: 2576-8484
Vol. 9, No. 2: 2208-2223, 2025
DOI: 10.55214/25768484.v9i2.5058

various penetration depths. All the samples have the same trend (BPbF0, BPbF5, BPbF10, BPbF15, and BPbF20). The EBF values depicted in Figure 9 were the lowest due to the complete absorption or removal of photons through photoelectric absorption.. Furthermore, two strong peaks in EBF values were discovered at around 20 KeV and approximately 60 MeVenergies, as illustrated in Figure 9. The first peak corresponds to Pb L1-edge absorption (about

15.8 keV), whereas the second corresponds to Pb k-edge absorption (around 88.0 keV). For significant penetration depths, the EBF values grow with more penetration depth due to many scattering events.

EBF values increases by increase the energy more than 2 MeV and for more mean free paths, this due to the pair production process which generate electrons and positrons. At lower penetration depths (0.5, 5, and 10 mean free paths), electron and positron pairs may gain enough kinetic energy to escape from the glass sample. However, at greater depths (20, 30, and40 mean free paths), these pairs are more likely to lose their energy within the thicker sample and come to rest, resulting in annihilation. This annihilation process generates two gamma photons (0.511 MeV) emitted in opposite directions. As a result, pair production can producelower-energy photons, causing an increase in EBF values at greater penetration depths [32]. At approximately 1 MeV, Compton scattering becomes the dominant interaction process forphotons. As a result, scattered (secondary) photons accumulate in the beam, resulting in abuildup within this energy range [30].

4. Conclusions

The study purpose is creating a new set of glass with the composition of $xPbF_2$-20Na_2O-10CaO-(70-x) B_2O_3, where the x takes the values (x = 0, 5, 10, 15, 20, and 25 mol.%). The effects of adding PbF_2 in borate glass on its physical and shielding properties were examined. The results revealed that.

- The increase of density of the glass samples with increasing the PbF_2 content, is attributed to the replacement of B_2O_3 whose molecular weight of (69.62 g/mole) and density of (2.46 g/cm3), with PbF_2 whose higher molecular weight of (245.196 g/mole) and higher density of (8.445 g/cm3). As B_2O_3 with low molecular weight is replaced by PbF_2 with high molecular weight, the glass system becomes more and more dense.
- The linear increase in the molar volume of the prepared glasses from 26.950 to 27.138 cm^3/mole can be attributed to the production of non-bridging oxygen atoms (NBO), which expands in turn the structure of the network of lead fluoride-borate glass network.
- The XRD confirms our prepared glass is an amorphous material.
- The prepared samples have excellent Gamma ray radiation shielding properties such as the mass attenuation coefficient, half value layer, mean free path, the effective atomic number and the effective neutrons number.
- The shielding properties of the prepared glass system is batter than the shielding properties of some concretes like the barite concrete, the shielding commercial glass like RS-360 and some earlier glass systems.
- The BPbF25 sample exhibits the most effective gamma-ray shielding properties.

In summary, the glass composition we prepared is well-suited for various radiation shielding applications, such as transparent windows in medical radiation devices, reactors, and handling radioactive waste.

Transparency:

The authors confirm that the manuscript is an honest, accurate, and transparent account of the study; that no vital features of the study have been omitted; and that any discrepancies from the study as planned have been explained. This study followed all ethical practices during writing.

Edelweiss Applied Science and Technology
ISSN: 2576-8484
Vol. 9, No. 2: 2208-2223, 2025
DOI: 10.55214/25768484.v9i2.5058

References
[1] P. Limkitjaroenporn, J. Kaewkhao, P. Limsuwan, and W. Chewpraditkul, "Physical, optical, structural and gamma-ray shielding properties of lead sodium borate glasses," *Journal of Physics and Chemistry of Solids*, vol. 72, no. 4, pp. 245-251, 2011. https://doi.org/10.1016/j.jpcs.2011.01.007

[2] K. Kirdsiri, J. Kaewkhao, A. Pokaipisit, W. Chewpraditkul, and P. Limsuwan, "Gamma-rays shielding properties of xPbO:(100− x) B2O3 glasses system at 662 keV," *Annals of Nuclear Energy*, vol. 36, no. 9, pp. 1360-1365, 2009. https://doi.org/10.1016/j.anucene.2009.06.019

[3] N. Singh, K. J. Singh, K. Singh, and H. Singh, "Comparative study of lead borate and bismuth lead borate glass systems as gamma-radiation shielding materials," *Nuclear Instruments and Methods in Physics Research Section B: Beam Interactions with Materials and Atoms*, vol. 225, no. 3, pp. 305-309, 2004. https://doi.org/10.1016/j.nimb.2004.05.016

[4] A. Abouhaswa, R. El-Mallawany, and Y. Rammah, "Direct influence of La on structure, optical and gamma-ray shielding properties of lead borate glasses," *Radiation Physics and Chemistry*, vol. 177, p. 109085, 2020. https://doi.org/10.1016/j.radphyschem.2020.109085

[5] A. Wagh, Y. Raviprakash, and S. D. Kamath, "Gamma rays interactions with Eu2O3 doped lead fluoroborate glasses," *Journal of Alloys and Compounds*, vol. 695, pp. 2781-2798, 2017. https://doi.org/10.1016/j.jallcom.2016.11.330

[6] M. Al-Buriahi *et al.*, "The role of PbF2 on the gamma-ray photon, charged particles, and neutron shielding prowess of novel lead fluoro bismuth borate glasses," *Journal of Materials Science: Materials in Electronics*, vol. 33, no. 3, pp. 1123-1139, 2022. https://doi.org/10.1007/s10854-021-07382-4

[7] H. Doweidar, K. El-Egili, and A. Altawaf, "Structural units and properties of BaF2–PbF2–B2O3 glasses," *Journal of Non-Crystalline Solids*, vol. 464, pp. 73-80, 2017. https://doi.org/10.1016/j.jnoncrysol.2017.03.023

[8] R. Nagaraju, K. C. Sekhar, M. Shareefuddin, L. Haritha, G. Lalitha, and K. V. Kumar, "Influence of ZnF2/PbF2 on physical and structural characteristics of bismuth borate glasses reinforced with chromium ions," *Optik*, vol. 247, p. 168028, 2021. https://doi.org/10.1016/j.ijleo.2021.168028

[9] H. Doweidar, G. El-Damrawi, and M. Abdelghany, "Structure–properties correlations in PbF2–B2O3 glasses," *Physics and Chemistry of Glasses-European Journal of Glass Science and Technology Part B*, vol. 55, no. 3, pp. 121-129, 2014. https://doi.org/10.13036/17533562.55.4.167

[10] M. Soraya, F. B. Ahmed, and M. Mahasen, "Enhancing the physical, optical and shielding properties for ternary Sb2O3–B2O3–K2O glasses," *Journal of Materials Science: Materials in Electronics*, vol. 33, no. 28, pp. 22077-22091, 2022. https://doi.org/10.1007/s10854-022-08971-7

[11] A. Ghanem and A. E.-S. Ahmed, "Effect of Sb2O4 on structural, physical and optical properties of sodium zinc borate glasses," *Egyptian Journal of Physics*, vol. 50, no. 1, pp. 1-11, 2022. https://doi.org/10.21608/ejphysics.2021.49672.1059

[12] Y. Abdelghany, M. Kassab, M. Radwan, and M. Abdel-Latif, "Borotellurite glass system doped with ZrO2, potential use for radiation shielding," *Progress in Nuclear Energy*, vol. 149, p. 104256, 2022. https://doi.org/10.1016/j.pnucene.2022.104256

[13] E. Şakar, Ö. F. Özpolat, B. Alım, M. Sayyed, and M. Kurudirek, "Phy-X/PSD: development of a user friendly online software for calculation of parameters relevant to radiation shielding and dosimetry," *Radiation Physics and Chemistry*, vol. 166, p. 108496, 2020. https://doi.org/10.1016/j.radphyschem.2019.108496

[14] M. S. Al-Buriahi and B. T. Tonguc, "Mass attenuation coefficients, effective atomic numbers and electron densities of some contrast agents for computed tomography," *Radiation Physics and Chemistry*, vol. 166, p. 108507, 2020. https://doi.org/10.1016/j.radphyschem.2019.108507

[15] Y. Abdelghany, M. Kassab, and M. Radwan, "Investigation of optical, mechanical, and shielding properties of zirconia glass capsule," *Progress in Nuclear Energy*, vol. 154, p. 104457, 2022. https://doi.org/10.1016/j.pnucene.2022.104457

[16] M. Al-Buriahi, C. Eke, Z. Alrowaili, A. M. Al-Baradi, I. Kebaili, and B. Tonguc, "Optical properties and radiation shielding performance of tellurite glasses containing Li2O and MoO3," *Optik*, vol. 249, p. 168257, 2022. https://doi.org/10.1016/j.ijleo.2021.168257

[17] M. Al-Buriahi, C. Eke, S. Alomairy, C. Mutuwong, and N. Sfina, "Micro-hardness and gamma-ray attenuation properties of lead iron phosphate glasses," *Journal of Materials Science: Materials in Electronics*, vol. 32, no. 10, pp. 13906-13916, 2021. https://doi.org/10.1007/s10854-021-05966-8

[18] N. A. Alsaif, Y. Rammah, I. Olarinoye, E. M. Ahmed, and A. Abouhaswa, "B2O3/PbO/Na2O/MgO/Nb2O5 glasses: Fabrication, physical, optical characteristics as well as photons/neutrons/beta particles attenuation capacities," *Optical and Quantum Electronics*, vol. 54, no. 9, p. 588, 2022. https://doi.org/10.1007/s11082-022-03990-4

[19] P. Kaur, K. Singh, S. Thakur, P. Singh, and B. Bajwa, "Investigation of bismuth borate glass system modified with barium for structural and gamma-ray shielding properties," *Spectrochimica Acta Part A: Molecular and Biomolecular Spectroscopy*, vol. 206, pp. 367-377, 2019. https://doi.org/10.1016/j.saa.2018.08.038

[20] R. Lebullenger, L. A. d. O. Nunes, and A. C. Hernandes, "Properties of glasses from fluoride to phosphate composition," *Journal of Non-Crystalline Solids*, vol. 284, no. 1-3, pp. 55-60, 2001. https://doi.org/10.1016/S0022-3093(01)00379-9

[21] B. Speit, "Radiation-shielding glasses providing safety against electrical discharge and being resistant to discoloration," U.S. Patent No. 5,073,524. U.S. Patent and Trademark Office. https://patents.google.com/patent/US5073524A, 1991.

[22] K. Singh, N. Singh, R. Kaundal, and K. Singh, "Gamma-ray shielding and structural properties of PbO–SiO2 glasses," *Nuclear Instruments and Methods in Physics Research Section B: Beam Interactions with Materials and Atoms*, vol. 266, no. 6, pp. 944-948, 2008. https://doi.org/10.1016/j.nimb.2007.11.069

[23] H. Gökçe, O. Güngör, and H. Yılmaz, "An online software to simulate the shielding properties of materials for neutrons and photons: NGCal," *Radiation Physics and Chemistry*, vol. 185, p. 109519, 2021. https://doi.org/10.1016/j.radphyschem.2021.109519

[24] N. A. Alsaif *et al.*, "Calculating photon buildup factors in determining the γ-ray shielding effectiveness of some materials susceptible to be used for the conception of neutrons and γ-ray shielding," *Journal of Materials Research and Technology*, vol. 11, pp. 769-784, 2021. https://doi.org/10.1016/j.jmrt.2021.01.052

[25] P. S. Singh, T. Singh, and P. Kaur, "Variation of energy absorption buildup factors with incident photon energy and penetration depth for some commonly used solvents," *Annals of Nuclear Energy*, vol. 35, no. 6, pp. 1093-1097, 2008. https://doi.org/10.1016/j.anucene.2007.11.009

[26] Y. Harima, "An historical review and current status of buildup factor calculations and applications," *Radiation Physics and Chemistry*, vol. 41, no. 4-5, pp. 631-672, 1993. https://doi.org/10.1016/0969-806X(93)90206-5

[27] Y. Harima, "An approximation of gamma-ray buildup factors by modified geometrical progression," *Nuclear Science and Engineering*, vol. 83, no. 2, pp. 299-309, 1983. https://doi.org/10.13182/NSE83-299

[28] Y. Harima, Y. Sakamoto, S.-i. Tanaka, and M. Kawai, "Validity of the geometric-progression formula in approximating gamma-ray buildup factors," *Nuclear Science and Engineering*, vol. 94, no. 1, pp. 24-35, 1986. https://doi.org/10.13182/NSE94-24

[29] R. El-Mallawany, *Radiation shielding properties of tellurite glasses. In Tellurite Glass Smart Materials: Applications in Optics and Beyond*. Amsterdam: Elsevier, 2018, pp. 17-27.

[30] Y. Rammah, I. Olarinoye, F. El-Agawany, and A. El-Adawy, "The impact of PbF2 on the ionizing radiation shielding competence and mechanical properties of TeO2–PbF2 glasses and glass-ceramics," *Ceramics International*, vol. 47, no. 2, pp. 2547-2556, 2021. https://doi.org/10.1016/j.ceramint.2020.09.100

[31] Y. B. Saddeek, E. R. Shaaban, and H. M. Moustafa, "Spectroscopic properties, electronic polarizability, and optical basicity of Bi2O3–Li2O–B2O3 glasses," *Physica B: Condensed Matter*, vol. 403, no. 13-16, pp. 2399-2407, 2008. https://doi.org/10.1016/j.physb.2008.01.005

[32] D. Gaikwad *et al.*, "Physical, structural, optical investigation and shielding featuresof tungsten bismuth tellurite based glasses," *Journal of Non-Crystalline Solids*, vol. 503, pp. 158-168, 2019. https://doi.org/10.1016/j.jnoncrysol.2018.09.038